

Author



Aaron Abajian has devoted his undergraduate research experience to developing computer tools for use in biology. For this project, under the mentorship of Professor Lowengrub, Aaron has combined the fields of computer science, biology and mathematics to create a unique mathematical tumor model. He has found the novelty of his project particularly exciting, especially as it has helped him truly understand many difficult concepts for the first time. Aaron is currently enrolled in a Credential and Master's Program in Urban Education at Loyola Marymount University, while teaching high school as part of the Teach for America Program.

Key Terms

- ◆ Agent-Based Model
- ◆ Computational Biology
- ◆ Continuous Model
- ◆ Mathematical Modeling
- ◆ Tumor Development

An Agent-Based Hybrid Model for Avascular Tumor Growth

Aaron C. Abajian

Biological Sciences, Computer Science & Engineering, and Mathematics

Abstract

Tumor development is a complex and multi-faceted process that cannot be captured in a single formula, yet the ability to predict a maturing tumor's magnitude and direction of growth would provide significant clinical benefits. *In-vitro* trials provide only limited predictive data since it is nearly impossible to chemically reproduce the exact environmental conditions surrounding a tumor. Moreover, each trial is necessarily unique to a specific tumor and cannot be quickly modified to satisfy the requirements of another. Mathematical models provide a virtual solution to this problem by implementing the core processes of tumor development in software. We present a model for tumor development from the single-cell stage to early microinvasion. An overlying nutrient field determines a cell's status as living, quiescent, mutant, or nonviable. Interactions between tumor cells are simulated using a competing exponential function and nutrient influx is modeled using the diffusion equation. The object-oriented implementation allows the introduction of multiple nutrient and chemical fields. The model may be applied to a variety of emerging tumors by carefully defining the constants that determine the tumors' development pathway and microenvironment. We present simulation results that demonstrate the flexibility of the model and its future applicability.

Faculty Mentor



This research introduces an agent-based model for simulating solid tumor growth. Mathematical modeling and numerical simulation have the potential to provide important insight into the root causes of solid tumor invasion and metastasis. Such models have been widely used for healthy cells but not for cancer modeling; however, the mechanisms are thought to be similar. An important feature of cancer is the communication and adhesion among the cancer cells and the extracellular matrix. At the time this research was performed, previous agent-based models did not consider this effect. Now, several other models account for these effects, although none consider the questions asked here. Research projects such as this provide undergraduates with a unique opportunity to bridge classroom experience and knowledge with important real world applications.

John S. Lowengrub

School of Physical Sciences

Introduction

Cancer

Cancer afflicted a reported 1.44 million individuals within the United States during 2007 (American Cancer Society 1). These cases encompassed the majority of organ systems in the human body. In each case, tumor development occurs along a characteristic pathway, yet effective treatment options are often limited by the type and location of the tumor. Generalized chemotherapeutic agents combat a broader selection of cancers by targeting the characteristic behaviors commonly seen in abnormal tissue.

The largest class of chemotherapeutic medications counters tumor cells that are overactive consumers. The mutations leading to the development of a tumor cell are often located in growth or proliferation genes and consequently induce the cell to rapidly consume nutrients within its vicinity (Hanahan and Weinberg 63). A toxic agent introduced into the patient's body is globally absorbed, but at a faster rate by cells mutant for the consumption gene. The rate of consumption of a particular substance depends on cellular phenotypes and the extracellular environment. These parameters must be considered when defining an appropriate dosage for a chemotherapeutic agent. The optimal solution would be dosage sufficient to eradicate the zealous tissue while exhibiting little to no harmful effect on the nearby normal tissue.

This seemingly complex problem may be reduced to a two-variable system involving the competition between the rate of drug diffusion in solution and the rate of cellular uptake. The former may be measured *in vitro* while the latter depends on a cell's phenotype. The rate of uptake by normal cells is expected to be less than that of mutant cells. The modeling challenge is to describe the rate of consumption of chemotherapeutic agents as a function of the tumor mass at any given time. A comparison may then be made against the basal uptake rate by normal tissue to determine the sufficient dosage for a tumor at its current stage. The uptake rate of a tumor at a given stage is clearly the result of its development pathway.

Tumor Development

The development of an invasive tumor from normal tissue is an elaborate process that roughly divides into three stages. Stage 1—A healthy cell must first accumulate a collection of mutations in a specific family of genes. The mutant cell then becomes the ancestral parent of a strain of mutated cells that forms a spherical mass isolated from the surrounding tissue. Stage 2—Peripheral tumor cells deplete the nutri-

ent supply as it diffuses into the spherical tumor. Central tumor cells are nutrient deprived resulting in a characteristic necrotic core. The tumor continues to thrive through the rapid division of viable cells on the sphere periphery. Stage 3—Environmental factors signal the peripheral cells to invade the surrounding tissue and/or to release chemical agents that induce the formation of nearby blood vessels. Metastasis of the tumor occurs locally (microinvasion) through individual cell movement or system-wide (macroinvasion) through the bloodstream.

Accumulation of Mutations. Tumor development begins when a single cell accumulates mutations in a set of critical genes. Several mutations are usually necessary to affect the change from normal to abnormal growth. The essential sets of genes implicated in tumor development are the tumor suppressor and oncogene families. These genes code for proteins that control cell proliferation and growth. A loss-of-function mutation in a tumor suppressor gene or a gain-of-function mutation in an oncogene may increase the division rate or the lifespan of the affected cell. A cell that proliferates incessantly or that ignores signals from other cells (esp. apoptotic signals) may give rise to a lineage of invasive cells.

Necrotic Core Formation. The rapid division of the initial mutant cell results in the logistic growth of a spherical tumor. Studies have indicated that, although tumor cells do not respond to signals from normal cells, they do exhibit adhesion to one another (Anderson 164). The close proximity of highly competitive cells results in the depletion of the local nutrient concentration. Cells stranded in the center of a tumor mass are starved for nutrients and form a necrotic central region. The tumor displays the characteristic three-layer structure of viable, quiescent and necrotic cells as a dynamic equilibrium is reached between diffusive nutrient influx and cellular nutrient consumption (Gerlee and Anderson 4).

Invasion. The starvation of inner tumor cells leads to their competitive advance. These cells may encroach upon the surrounding tissue or release signaling molecules that promote the growth of nearby blood vessels. Microinvasive encroachment is a localized phenomenon that is performed by phenotypically mutant cells. The mutation allows the cells to successfully detach from the spherical tumor mass. A macroinvasive cell may release Vascular Endothelial Growth Factors (VEGFs) that induce endothelial cells to form vessels towards the tumor. VEGFs are signaling proteins that normally play benign roles but also function as an abnormal cell's response to nutrient deprivation. The pro-

cess by which tumor cells gain access to the blood supply is termed vascularization.

Mathematical Models

The three stages of tumor development are the result of complex intracellular, intercellular and extracellular processes. The inherent difficulty of reducing each stage into scientifically useful pieces has given rise to sophisticated tumor models. The goal of an abstract model is to understand a complex system that cannot be appreciated using the typical pen-and-paper approach. In biology, the existence of multiple inhibitors and repressors for a single gene provides an immediate appreciation for the utility of a calibrated model. An initial concentration and spatial distribution may be specified for each enzyme and the resulting gene activity calculated without *in-vitro* experimentation (Jiang et al. 3885). Similarly, a thoroughly developed tumor model could provide preemptive information about a tumor’s development pathway. Models aiming to achieve this goal are still in their infancy and are broadly classified as either continuous or discrete. Models that incorporate features from both classes are termed hybrid models.

Continuous Models. A continuous model is defined by partial differential equations (PDEs) that govern the evolution of a tumor mass. The tumor’s physical dimensions and growth rate are measured and visually displayed without reference to the behavior of the underlying cells. Continuous models sacrifice the maintenance of cell-specific properties in favor of computational speed.

Discrete Models. Portions of a discrete model may be based on continuous PDEs, but the heart of a discrete model is the maintenance of disjoint units of information that change over time and sum to produce the overall system. Time is broken into constant steps rather than allowing for a continuous progression. For example, an agent-based discrete model may focus on the individual objects affecting a system’s evolution. An agent-based population model would store location and genotypic/phenotypic information for every member of the species within the region of interest. Population trends would be calculated based on the pairwise interactions between individuals over time, rather than an overall PDE describing the population mass. This modeling approach is computationally demanding but provides greater insight into the constructed nature of the system.

Hybrid Models. A combination of continuous and discrete modeling techniques provides the benefits of both implementations within the same simulation (Ramis-Conde, Chaplain, and Anderson 534). A discrete model for the

distribution of bacteria after exposure to an antibiotic could model individual cells by biasing their proliferation and viability according to the drug’s spatial distribution. This agent-based model could be extended by incorporating the continuous diffusion equation to describe the movement of the antibiotic down its concentration gradient. The resulting hybrid model would simulate the bacteria’s response to a diffusing antibiotic in solution.

Mathematical Model

We present avascular tumor development using a two-dimensional hybrid continuum/discrete mathematical approach. Our model simulates the development pathway from a single cell to the formation of a stable necrotic region and proceeds to the early stages of microinvasion. Cells function as the component agents whose properties are maintained. Stored cell data includes spatial, genotypic and phenotypic information. The diffusion PDE is used to model the competition between diffusive nutrient influx

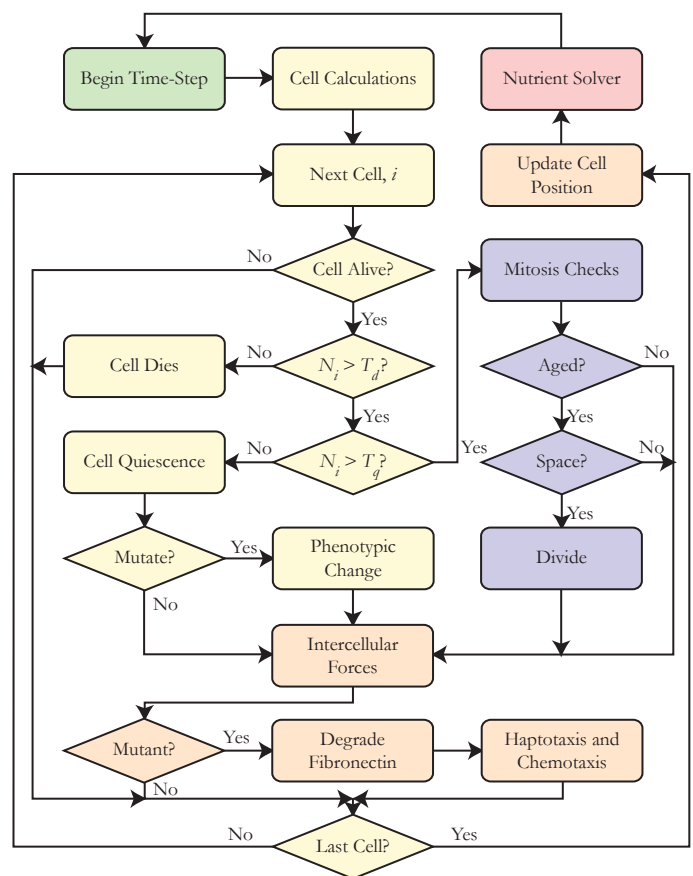


Figure 1
Overall simulation flowchart. The symbol N_i denotes the nutrient concentration around cell i . T_d refers to the viability threshold while T_q refers to the quiescence threshold.

and cellular nutrient uptake. Tumor cells adhere to and repel from one another via the potential interaction equation previously described by Chuang et al. (Li Chuang, et al. 4). Temporal progression occurs through discretized time-steps. Figure 1 provides an overview of the processes that occur within a single time-step.

A common set of calculations is performed on the cells during each time-step. These calculations include routine tasks such as verifying viability and quiescence statuses (yellow blocks) and checking for mitosis (blue blocks). The lower orange blocks in Figure 1 refer to processes that affect cellular movement. These processes include intercellular forces, haptotaxis and chemotaxis. Cell positions are updated after the last iteration through the loop. The nutrient concentration described by the PDE is allowed to reach equilibrium prior to the next time-step (red block).

Cell Calculations

The model maintains a set of physical variables for each cell. Table 1 provides a list of these properties along with their default values as specified for the initial cell. The values of these properties collectively determine the cells' division, localized movement and invasion rates during each time-step.

Table 1

List of viability parameters maintained for every cell along with their non-dimensionalized default values

Variable	Initial Value
Speed	1.000
Age	0.000
Time until next cell division	0.083
Mitosis period	0.083
Lifespan	∞
Generation Number	0.000
Maximum Generation	∞
Current position in space	(0, 0, 0)
Local nutrient concentration	1.000
Quiescent	No
Contains phenotypic mutation	No
Living	Yes

Physical Variables. A cell remains alive and capable of dividing as long as there is sufficient nutrient in its vicinity. If the local nutrient concentration drops below the quiescence threshold, T_q , the cell loses its ability to divide. Quiescent cells have a slower metabolic rate that is modeled by a decreased rate of nutrient consumption. Microinvasive

tumor cells arise from quiescent cells undergoing extreme nutrient deprivation. If the nutrient concentration falls below the viability threshold, T_b , the cell dies.

The starvation of tumor cells has been implicated in the microinvasion pathway. We model this phenomenon by inducing a phenotypic mutation in randomly chosen quiescent cells. A phenotypically modified cell detaches from the tumor mass and migrates up the nutrient gradient by degrading the local fibronectin concentration.

Mitosis. A cell undergoes mitosis if several conditions are met. First, the cell must not be quiescent or a phenotypic mutant as determined by the previous checks. There is also a minimum waiting period after the cell's previous division. This check ensures that the cell has had enough time to perform the essential stages of the cell cycle. The waiting period for division is dependent on the local nutrient concentration. This models the increased time it takes a cell to acquire sufficient resources to divide in a nutrient-deficient environment.

The last mitosis check verifies that there is sufficient space around the parent cell. Physically, a cell cannot divide when it is spatially constrained by adjacent cells. This phenomenon is taken into account by examining the cell's repulsion coefficient from the potential interactions equation. The repulsion coefficient must be below a constant threshold to permit division. A cell that passes all of the checkpoints divides into two daughter cells. A new cell is added to the cell array with identical parameters to that of the parent except for location. The new cell's position is a small random offset of the parent's position.

Cell Movement

Selected cells move a random amount according to the Gaussian Normal Distribution with mean zero and standard deviation equal to the square of the time-step size. These cells also move in response to the forces exerted on them by nearby cells and in response to chemical and nutrient gradients. These biasing agents influence the velocity of a cell. In general, we may express the continuous position of a cell at time t as:

$$\bar{x}(t) = \int_0^t \bar{v}(s) ds \quad (1)$$

Where $\bar{v}(t)$ is the velocity vector of the cell at time t . To discretize this formula, suppose that we wish to update a cell's position for the n th time-step given that we are on time-step $n - 1$. We may split the integral along this time:

$$\bar{x}(n\Delta t) = \overbrace{\int_0^{(n-1)\Delta t} \bar{v}(s) ds}^{\text{Cell position at time-step } (n-1)} + \overbrace{\int_{(n-1)\Delta t}^{n\Delta t} \bar{v}(s) ds}^{\text{Displacement of cell during } n\text{th time-step}} \quad (2)$$

Note that Δt in this case denotes the size of one time-step. The first integral represents the cell's position at time-step $n - 1$:

$$\bar{x}(n\Delta t) = \bar{x}((n-1)\Delta t) + \int_{(n-1)\Delta t}^{n\Delta t} \bar{v}(s) ds \quad (3)$$

For sufficiently small Δt , we may approximate the right integral by the product $\bar{v}(n\Delta t)\Delta t$:

$$\bar{x}(n\Delta t) = \bar{x}((n-1)\Delta t) + \bar{v}(n\Delta t)\Delta t \quad (4)$$

This is the discretized formula for calculating a cell's position at time $n\Delta t$ given the cell's position at the previous time-step. The value of the velocity vector at time $n\Delta t$ is determined by the sum of velocity vectors from each biasing agent:

$$\bar{v} = D_I \bar{v}_I + D_H \bar{v}_H + D_C \bar{v}_C \quad (5)$$

The subscripts I, H and C stand for intercellular interactions, haptotaxis and chemotaxis, respectively. D_X is a constant coefficient defined for biasing agent X . The velocity components are described in detail in the following sections.

Intercellular Forces. Cell-to-cell adhesion and repulsion mutually contribute to the intercellular forces term in the velocity equation. For each pair of cells located at \bar{x}_i and \bar{x}_j we define the interaction potential to be:

$$U_{i,j} = \overbrace{C_A e^{-\frac{|\bar{x}_i - \bar{x}_j|}{L_A}}}^{\text{Attraction}} - \overbrace{C_R e^{-\frac{|\bar{x}_i - \bar{x}_j|}{L_R}}}^{\text{Repulsion}}$$

Where C_A and C_R are magnitude constants of attraction and repulsion, and L_A and L_R are length-scale constants of attraction and repulsion. A positive value of U indicates an attractive potential between the pair of cells while a negative value represents a repulsive potential. A potential value of zero indicates that the cells are at an equilibrium distance apart. The gradient of the potential function provides the direction that one cell must move to reach equilibrium with the other cell. The sum of the potential gradients from all other cells determines the intercellular forces velocity term for cell i :

$$\bar{v}_I^i = \sum_{j=1, j \neq i}^{N(t)} \nabla U_{i,j} \quad (6)$$

The value of $N(t)$ is the number of cells at time t . The strength of adherence and repulsion are examples of cell-specific constants that can be maintained in an agent-based model.

Haptotaxis and Chemotaxis. Phenotypically mutant cells invade to replenish their depleted nutrient supply. Movement occurs upwards along the nutrient gradient via the degradation of extracellular matrix (ECM) proteins. We model the ECM protein, fibronectin, through the use of a square lattice of chemical grid points similar to the angiogenesis model of Plank and Sleeman (Plank and Sleeman 1798). Migrating mutant cells simultaneously produce fibronectin to form channels exiting the tumor. Thus, although nutrient deprived cells must climb the fibronectin scaffold to exit the tumor, they replenish it with a higher concentration of protein. Future mutated cells tend to follow the previously taken pathways due to the higher fibronectin concentration.

As noted above, the concentration of fibronectin at a mutant cell's position directly affects the rate of movement due to the nutrient gradient. Considering cell i located at \bar{x}_i we have:

$$\bar{v}_C^i = f_{\bar{x}_i} \nabla u_{\bar{x}_i} \quad (7)$$

The symbols f and u represent the fibronectin and nutrient fields, respectively, and thus $f_{\bar{x}_i}$ and $u_{\bar{x}_i}$ are the values of these fields at the cell's position during the current time-step. The fibronectin field increases slowly as mutant cells progress away from the tumor. In addition to increasing the mobility of starved cells along the nutrient gradient, the newly created fibronectin channels increase the rate at which cells move down the fibronectin gradient.

Migrating cells choose pathways with the highest availability of ECM proteins. We model this phenomenon by introducing a haptotaxis biasing agent that influences cells to move along the fibronectin gradient:

$$\bar{v}_H^i = \nabla f_{\bar{x}_i} \quad (8)$$

Nutrient Field

The model simulates a single nutrient field across the square computation plane. Nutrient flows inward according to the diffusion equation with a fixed boundary of one. Living cells consume the nutrient field at an exponential rate. The consumption rate is highly localized around each cell and falls off quickly with distance. Equation 9 presents the nutrient PDE in its entirety.

$$\frac{\partial u}{\partial t} = \overbrace{k \nabla^2 u}^{\text{Nutrient Diffusion}} - \overbrace{\left(\sum_{l=1}^{N(t)} f(u, \bar{x}_l) \right)}^{\text{Nutrient Consumption}} \quad (9)$$

Nutrient Diffusion

The nutrient concentration is replenished according to the diffusion equation in two dimensions with a fixed square boundary:

$$k \nabla^2 u = k \left(\frac{\partial^2 u}{\partial x^2} + \frac{\partial^2 u}{\partial y^2} \right) \quad (10)$$

The constant k determines the rate of nutrient influx. The diffusion rate of oxygen in water varies strongly with temperature. At 20 °C, the coefficient k has been previously calculated as 0.00197 mm²/s (Richard 1)

Nutrient Consumption. Cells consume nutrient at a rate that falls off exponentially with distance. The summation in Equation 9 is over the set of living cells at time t . Cell l consumes the local nutrient according to the following equation:

$$f(u, \bar{x}_l) = -\lambda e^{-\frac{\varepsilon - \bar{x}_l^2}{\varepsilon^2}} u \quad (11)$$

Where λ is the single-cell consumption rate, \bar{x}_l is the location of cell l as a function of time, and ε sets the degree of localized nutrient consumption.

Numerical Methods

The agent-based modeling paradigm strongly supports an object-oriented implementation. We view cells as self-contained entities with a fixed set of physical characteristics and functions (division, invasion, interactions, etc.). In an object-oriented programming language, information unique to a particular class of objects, such as cells, may be encapsulated and protected from external modification. We refer to implemented classes using an italicized term with the first letter of each word capitalized to distinguish them from their physical analogues (e.g. *Cell* refers to the class representing a physical cell). The process of instantiation creates an object of the respective class and allocates memory to store the new object's data. Thus, instantiation of the *Cell* class performs the necessary tasks to create a new cell. A complete list of the classes implemented in the model is provided in Table 2. Portions of the model implemented in each class are discussed in the section that follows.

The classes *NutrientEquation*, *PotentialInteractions* and *Fibronectin* inherit operations from the more general *GenericField* class. Inheritance is an important object-oriented programming concept that allows code to be reused among similar classes. Its use in the model provides a high degree of scalability.

Table 2

List of classes implemented in the model. An object-oriented implementation allows the encapsulation of data unique to a specific class of objects.

Class
<i>TumorGrowth</i>
<i>Cell</i>
<i>Mitosis</i>
<i>NutrientEquation</i>
<i>Fibronectin</i>
<i>DecayingFibronectin</i>
<i>PotentialInteractions</i>

The numerical tools used to implement the model were chosen based on their running time efficiency and ability to provide the desired object-oriented features. The model was written in C++ for rapid execution and real-time visualization. MATLAB was used for partial postprocessing visualization.

Implemented Classes

TumorGrowth. The *TumorGrowth* class maintains an array of *Cell* objects that is initially populated with a single cell. The class controls execution of the model by calling functions to perform the actions presented in the flow chart of Figure 1. Quick comparison calculations are carried out within *TumorGrowth* while more complex operations are located within their own classes (e.g. *Mitosis*, *NutrientEquation* and *PotentialInteractions*).

At every time-step, a subset of living cells from the cell array is selected for the calculation loop shown in Figure 1. Simulation results indicate that it is sufficient to take $\log_{10}(N)$ cells where N is the size of the cell array. This is primarily a consequence of the small time-step relative to the number of cells. In larger simulations, it would be necessary to choose a greater subset of cells.

The selected cells are passed to an update function that updates that cell's local nutrient concentration and checks it against the nutrient thresholds. The cell's quiescent, phenotypic mutation and living boolean variables are updated appropriately. Note that once a cell is marked as dead it is no longer a candidate for the update function. The update

function increments the cell's age variable and checks for mitotic cell division.

Cell and Mitosis. The *Cell* and *Mitosis* classes are strongly linked. After *TumorGrowth* verifies that a cell is ready to divide, it invokes an instance of *Mitosis* to perform the division. The division function copies all of the parent cell information and returns a new *Cell* object that is added to the array of cells.

NutrientEquation. The *NutrientEquation* class contains the numerical implementation of Equation 9. The nutrient concentration is defined across a rectangular grid of points. During each time-step of length t , nutrient diffuses across the nodes and cells consume from the nearby nodes. Discretization of the diffusion portion was accomplished using the central difference method. To begin the derivation of the nutrient concentration at node (i, j) and time-step $n + 1$, we first rewrite the left-most and right-most portions of Equation 9 as:

$$\frac{u_{i,j}^{n+1} - u_{i,j}^n}{\Delta t} = k \left(\frac{\partial^2 u}{\partial x^2} + \frac{\partial^2 u}{\partial y^2} \right)^n - \lambda \sum_{l=1}^{N(n\Delta t)} e^{-\frac{|x_i - x_j - \bar{x}_l(n\Delta t)|^2}{\epsilon^2}} u_{i,j}^n \quad (12)$$

Notice that we have substituted $n\Delta t$ in for the continuous time t since we are assuming a fixed time-step. The superscript n on the continuous diffusion term merely denotes that we are considering a discretized time-step.

The central difference method computes the gradient at a grid point by taking the average value of the gradient across the four nearest grid points. In particular, we may rewrite the continuous diffusion equation at time-step n as:

$$\left(\frac{\partial^2 u}{\partial x^2} + \frac{\partial^2 u}{\partial y^2} \right)^n = \frac{u_{i+1,j}^n - 2u_{i,j}^{n+1} + u_{i-1,j}^{n+1}}{\Delta x^2} + \frac{u_{i,j+1}^n - 2u_{i,j}^{n+1} + u_{i,j-1}^{n+1}}{\Delta y^2} \quad (13)$$

Substituting this expression into that of Equation 12 produces the completely discretized nutrient equation:

$$\frac{u_{i,j}^{n+1} - u_{i,j}^n}{\Delta t} = k \left(\frac{u_{i+1,j}^n - 2u_{i,j}^{n+1} + u_{i-1,j}^{n+1}}{\Delta x^2} + \frac{u_{i,j+1}^n - 2u_{i,j}^{n+1} + u_{i,j-1}^{n+1}}{\Delta y^2} \right) - \lambda \sum_{l=1}^{N(n\Delta t)} e^{-\frac{|(i,j) - \bar{x}_l(n\Delta t)|^2}{\epsilon^2}} u_{i,j}^n \quad (14)$$

The model uses a fixed spacing, h , between adjacent horizontal and vertical nodes so we have $\Delta x = \Delta y = h$. Equation

14 may be solved for the value of the nutrient concentration at grid point (i, j) and time-step $n - 1$:

$$u_{i,j}^{n+1} = \frac{k \left(u_{i+1,j}^n + u_{i-1,j}^{n+1} + u_{i,j+1}^n + u_{i,j-1}^{n+1} \right) + \gamma u_{i,j}^n - \lambda h^2 \sum_{l=1}^{N(n\Delta t)} e^{-\frac{|(i,j) - \bar{x}_l(n\Delta t)|^2}{\epsilon^2}} u_{i,j}^n}{\gamma + 4k} \quad (15)$$

Where $\gamma = \frac{h^2}{\Delta t}$. The initial nutrient concentration at each grid point is set to one: $u(x, y, 0) = 1$ and the boundary is fixed at one: $u(\min(x), y, t) = 1$, $(\max(x), y, t) = 1$, $(x, \min(y), t) = 1$, $(x, \max(y), t) = 1$.

An object of the *Nutrient* class maintains a discrete field of nutrient grid points along with functions for updating the field. Requests for evaluation at an arbitrary point on the computation plane are mapped to the nearest grid point. The competition between the influx of nutrient by diffusion and the removal of nutrient by cellular consumption stabilizes after several iterations. Only grid points whose nutrient values have changed significantly (defined by a constant) are updated. A single pass over all the grid points identifies those that have changed. The single pass is performed again after a set number of uptake cycles have occurred. This algorithm was first introduced by Dr. Paul Macklin and decreases the time needed to solve the discretized nutrient equation (Macklin and Lowengrub 283).

Fibronectin and DecayingFibronectin. The *Fibronectin* and *DecayingFibronectin* classes contain the necessary routines to maintain and update the discretized fibronectin field. The implementation is identical to that of the *NutrientField* class minus the diffusion functions. The *Fibronectin* class defines the underlying grid while the *DecayingFibronectin* class contains functions that cells call to create or diminish the field. The degradation and production functions for each cell are the same as Equation 11. Note, however, that the rate coefficients of nutrient degradation, fibronectin degradation and fibronectin production are distinct and that the production coefficient is negative.

PotentialInteractions. The task of calculating cellular interactions is passed off to a separate *PotentialInteractions* class. A member function of this class accepts a reference to the current cell array and a specific cell index. The function iterates over the array and computes the summation given in Equation 6. The attractive and repulsive components are computed independently and preserved in separate arrays. This is necessary for the cell-repulsion check prior to mitosis.

Field Inheritance

The *PotentialInteractions* class inherits functions from the more general *GenericField* class. The *Fibronectin* and *Nutrient* classes also inherit from *GenericField*. It is worth describing the structure of this inheritance to obtain a clear picture of the benefits of the object-oriented design of the model. Although the potential, nutrient and fibronectin fields conceptually represent distinct entities, the physical definition of a field implies certain common characteristics.

The situation of having two similar objects that share synonymous functions, but with different implementations, arises quite often in computer science. Inheritance allows a general description of the commonalities between the classes while maintaining enough room for separate implementations. *GenericField* provides function names for a physical field. Evaluation, the spatial partial derivatives, and the magnitude of the gradient are defined in *GenericField* (see Table 3 for a complete list of functions defined in *GenericField*). In fact, the magnitude of the gradient is implemented in *GenericField* although the partials themselves are not. Inheriting classes must implement functions not implemented in *GenericField* (i.e. everything but the gradient magnitude), but a common naming convention is preserved. In this manner, it is a trivial task to define an array of *GenericField* objects whose actual instantiations may be any of *PotentialInteractions*, *Nutrient* or *Fibronectin*.

Table 3

Functions defined in the *GenericField* class along with inheriting classes and the method of each implementation.

Abstract Class <i>GenericField</i>		
Function	Implementing classes and type of implementation	
$f(x, y, z)$	<i>PotentialInteractions</i>	Direct evaluation of Equation (6)
	<i>Fibronectin</i>	Discretized using the central difference method
	<i>Nutrient</i>	
$\frac{\partial f}{\partial x}, \frac{\partial f}{\partial y}, \frac{\partial f}{\partial z}$	<i>PotentialInteractions</i>	Continuous derivation from Equation (6)
	<i>Fibronectin Nutrient</i>	Discretized using the central difference method
$ \nabla f $	<i>GenericField</i>	Implemented as $\sqrt{\left(\frac{\partial f}{\partial x}\right)^2 + \left(\frac{\partial f}{\partial y}\right)^2 + \left(\frac{\partial f}{\partial z}\right)^2}$

Implementation Tools

Standard computational tools were used to construct the model. An object-oriented framework was built to support each cell as an autonomous unit. The entire simulation was written in C++ with strict adherence to accepted best-practices in class design. Independent classes were constructed to maintain the functions and parameters of cells, fields and other distinct entities within the model. Visualization was accomplished through an OpenGL-based display and frame-by-frame output. Cell data was also output as a text file containing each time-step. The latter enabled postprocessing visualization in MATLAB without the time-consuming process of concatenating image files. A simulation begins upon instantiation of the central *TumorGrowth* class.

4. Numerical Results

The simulation parameters in Tables 1 and 4 along with other parameters, such as those for the nutrient field and cellular interactions, determine the overall behavior of the tumor.

Table 4

List of global constants that determine the pathway of tumor development.

Global Constants	
Variable	Initial Value
Maximum number of cells	∞
Computation window dimensions	$[-1, 1] \times [-1, 1]$
Number of iterations	∞
Time-step size	0.001
Random number seed	1.000
Quiescence nutrient threshold	0.600
Living nutrient threshold	0.500
Mutation nutrient threshold	0.510
Repulsion maximum for division	2.000

Selected parameters were varied to understand their effects on the simulation. The five variables considered are listed in Table 5. Three thresholds exist that determine a tumor cell's status as normal, quiescent, mutant, or dead (see Figure 1). The images in Figures 2 through 7 represent these states as green, blue, black, and red, respectively. Phenotypic mutations were disabled in Figures 2, 3 and 4 to focus on the tumor at the stable necrosis stage prior to microinvasion.

Table 5
List of global constants that determine the pathway of tumor development.

Simulation Specific Constants		
Variable	Symbol	Default Value
Potential attraction/repulsion coefficient ratio	C_A/C_R	0.300
Potential attraction and repulsion length-scales	L_A, L_R	0.500, 0.100
Quiescence nutrient threshold	T_q	0.600
Living nutrient threshold	T_d	0.500
Mutation nutrient threshold	T_m	0.510

Potential Coefficients

The potential coefficients and length-scales are those given in Equation 6. The effect of the potential coefficients on the diameter of the tumor at a particular time-step is visu-

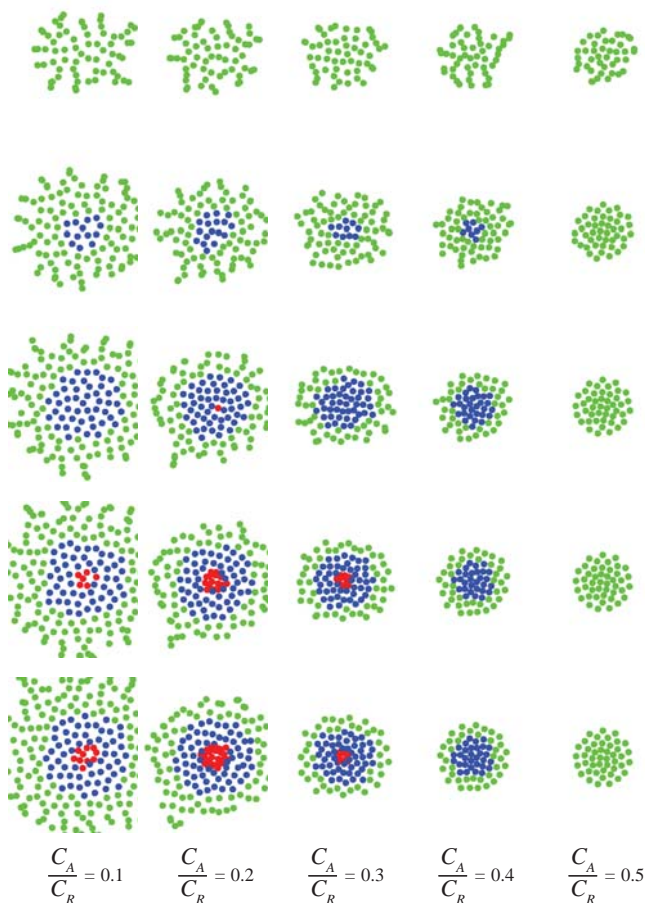


Figure 2
Effect of attraction/repulsion ratio on tumor diameter. The vertical axis is set up in one thousand time-step increments with the first row being at the thousandth step. The length-scales of attraction and repulsion have been set to 0.5 and 0.1, respectively.

ally demonstrated in Figure 2. Similarly, Figure 3 shows the effects of the length-scale on the tumor’s development. The tumor’s dimensions are largely determined by these four parameters. It is a requirement that the greater length-scale belong to the weaker force. This prevents implosion or indefinite expansion of the tumor.

Attraction to Repulsion Ratio. Increasing the ratio of attraction to repulsion increases the tendency of cells to adhere to one another. Lower values of C_A/C_R produce larger tumors suitable for simulations requiring thousands of cells. High values constrict the cells together reducing the diameter of the tumor. A small tumor diameter precludes cell division because of the adjacency check prior to division. The decreased number of cells prevents depletion of the nutrient and provides for cell viability.

Attraction and Repulsion Length-Scales. The potential length-scale constants determine the effective radii of attraction and repulsion. The computation plane consisted of the unit-square and the repulsion length-scale was fixed at one-tenth of this value. The left-most image of Figure 3 occurs when the length-scale of attraction equals that of repulsion. In this case, the tumor’s dimensions are determined by the ratio of the attraction and repulsion coefficients. The latter four images are similar because the attraction length-scale strongly dominates the repulsion length-scale, although the magnitude of localized repulsion is still greater.

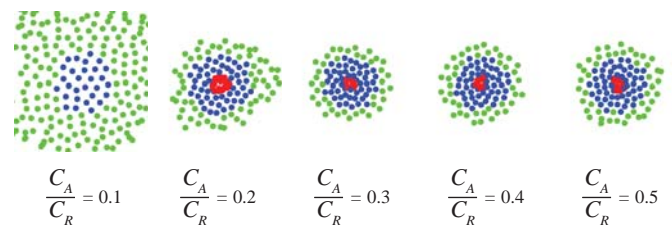


Figure 3
Effect of increasing the length-scale of attraction. The repulsion length-scale was fixed at 0.1 while the ratio of attraction to repulsion was set to 0.3. The images were taken at the five-thousandth time-step. The last four image are similar because the attraction length-scale strongly dominates the repulsion length-scale.

Nutrient Thresholds

Figures for the quiescence, viability, and mutation thresholds were produced at the five-thousandth time-step as still frames from the graphical output.

Quiescence. A cell must drop below the fixed T_q threshold to become quiescent. Figure 4 shows the effects of increasing T_q on the tumor. The number of cells in the quiescent

state increases with T_q thereby determining the depth of the viable rim.

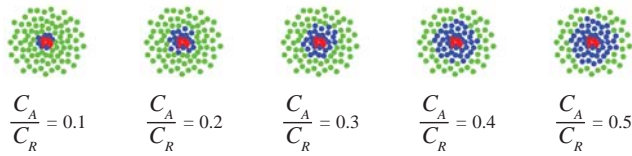


Figure 4
Effect of varying quiescent nutrient threshold, T_q , on tumor morphology.

Viability. Cells whose local nutrient concentration drops below the threshold for viability, T_d , are marked as dead. Figure 5 shows four simulations with increasing viability thresholds. A high viability threshold decreases the time a cell may exist in the quiescent state. Thus, the number of quiescent cells diminishes rapidly as the necrosis threshold is increased.

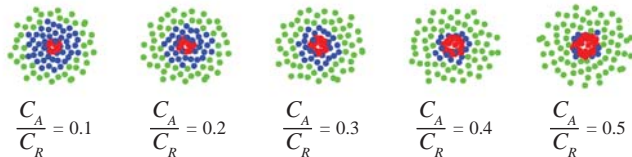


Figure 5
Effect of varying viability nutrient threshold, T_d , on tumor morphology.

Mutation. A subset of the cells that fall below the mutation threshold are made to undergo a microinvasive phenotypic mutation. Note that the mutation threshold, T_m , is less than T_q to ensure that the invading cells are mitotically deactivated due to nutrient deprivation. Figure 6 shows the effects of increasing the mutation threshold. The increasing mutation threshold decreases the number of necrotic cells since mutant cells are able to migrate away from the nutrient-deprived core.

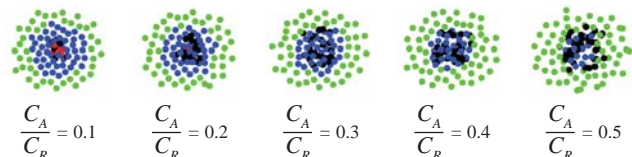


Figure 6
Effect of varying mutation nutrient threshold, T_m , on tumor morphology.

Over time, the mutant cells break the adhesive forces binding them to the other cells and move away from the tumor along fibronectin and nutrient gradients. Figure 7 shows a longer simulation at the forty-thousandth time-step. The darkened paths were produced by interpolating the fibronectin grid points across the pixels of the figure. The darker lines indicate a high fibronectin concentration.

Mutant cells degrade and produce the local fibronectin concentration. Production is the dominating process and thus mutant cells create pathways of high fibronectin as they leave the tumor. Later mutants tend to exit the tumor along these preformed paths.

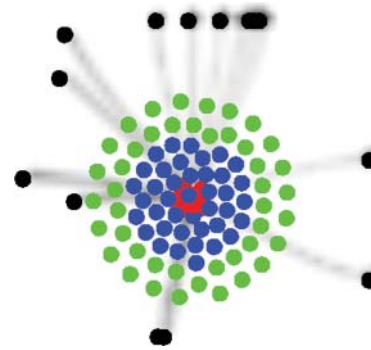


Figure 7
A fraction of viable cells below the mutant threshold are selected to undergo a phenotypic mutation. These cells move away from the tumor up the nutrient gradient. Each cell produces a local fibronectin field that also biases the motion of future mutants. This type of migration is termed microinvasion and is believed to be a response to nutrient deprivation. This still frame was taken at the forty-thousandth time-step.

Conclusion

An extensive range of processes participate in tumor development. The three generalized phases of tumor growth include the initial single-cell genetic mutation and exponential division, formation of a circular mass with a central necrotic region and a proliferating rim, and invasion on either a micro or macro level. Chemotherapeutic treatment options focus on the rampant proliferation and consumption associated with invasive tissue. The question of appropriate medicinal dosage rests on the rate of abnormal drug consumption compared to the basal consumption rate. We have introduced a computational model for avascular tumor growth that simulates the essential competition between diffusive nutrient influx and cellular nutrient uptake witnessed in a variety of tumors.

The model maintains individual cell data in an agent-based fashion while incorporating features of continuous models

to allow for nutrient flow. This structure provides unique insight into the pathway to necrotic core formation and microinvasion, especially in regards to competitive nutrient depletion. The model demonstrates a clear transition from a fully viable spherical mass to the commonly observed three-tiered tumor (i.e. viable rim, quiescent region and necrotic core). The model's parameters determine the width of these regions at the stability stage prior to invasion. The magnitude and length-scales of attraction and repulsion affect the overall size of the tumor while the nutrient thresholds specify the minimum concentration of resources necessary for viability, mutation and quiescence.

Although future work is necessary to determine the appropriate constants for specific cases, this model functions well as an initial tumor development framework. A substantive improvement would be the introduction of independent nutrient and chemical fields that influence cellular behavior. Immersion of the tumor model into such a simulated microenvironment that includes normal cells would provide immediate predictive ability about the appropriate substance concentration to establish a particular level of tumor necrosis. The model is well adapted to this endeavor through its scalable implementation of cells and chemical fields.

Acknowledgements

The author thanks Professor John Lowengrub for his relentless support and guidance. The author also gratefully recognizes the generous support of the Undergraduate Research Opportunities Program at UC Irvine and the Henry Samueli School of Engineering Undergraduate Research Fellowship.

Works Cited

- American Cancer Society, "Cancer Facts & Figures." 2007: 1–56.
- Anderson, A.R. "A hybrid mathematical model of solid tumour invasion: the importance of cell adhesion." *Math Med Biol* 22 (2005): 163–186.
- Gerlee, P. and A. R. A. Anderson. "Stability Analysis of a Hybrid Cellular Automaton Model of Cell Colony Growth." *Physical Review* 75 (2007): 051911.
- Hanahan, D. and R Weinberg. "The Hallmarks of Cancer." *Cell* 100(1) (2000): 57–70.
- Jiang, Y., et al. "A multiscale model for avascular tumor growth." *Biophys. J.* 89 (2005): 3884–3894.
- Li Chuang, Yao, et al. "State Transitions and the Continuum Limit for a 2D Interacting, Self-Propelled Particle System." 2006: 1–36.
- Macklin, P. and John S. Lowengrub. "A New Ghost Cell/Level Set Method for Moving Boundary Problems: Application to Tumor Growth." *Journal of Scientific Computing* 35 (2007): 266–299.
- Plank, M. J. and B. D. Sleeman. "Lattice and non-lattice models of tumor angiogenesis." *Bull. Math. Biol.* 66.6 (2004): 1785–1819.
- Ramis-Conde, Ignacio, Mark A.J. Chaplain, and Alexander R.A. Anderson. "Mathematical modeling of cancer cell invasion of tissue." *Math. and Comp. Model.* 47 (2007): 533–545.
- Richard, Tom. "Calculating the Oxygen Diffusion Coefficient in Water." 2005: <<http://www.css.cornell.edu/compost/oxygen/oxygen.diff.water.html>>.

